LIMNOLOGY and OCEANOGRAPHY

ASLO

Limnol. Oceanogr. 9999, 2024, 1–12

doi: 10.1002/lno.12723

Can intense storms affect sinking particle dynamics after the North Atlantic spring bloom?

Elisa Romanelli,[1*] **Sarah Lou Carolin Giering**,[2] **Margaret Estapa**,[3] **David A. Siegel**,[1] **Uta Passow**[1,4]

[1]Earth Research Institute, University of California, Santa Barbara, California, USA
[2]National Oceanography Centre, Southampton, UK
[3]School of Marine Sciences, Darling Marine Center, University of Maine, Walpole, Maine, USA
[4]Memorial University, St John's, Newfoundland and Labrador, Canada

Abstract

The sinking of large particles (i.e., marine snow) has long been recognized as a key pathway for efficient particulate organic carbon (POC) export to the ocean interior during the decline of spring diatom blooms. Recent work has suggested that particles smaller than marine snow can also substantially contribute to POC export. However, a detailed characterization of small and large sinking particles at the end of blooms is missing. Here, we separately collected suspended and small and large sinking particles using Marine Snow Catchers and assessed their biogeochemical composition after the North Atlantic spring bloom in May 2021. During the 3 weeks of sampling, when four intense storms (maximum wind speeds 37–50 kt) created high turbulent kinetic energy dissipation rates and deepened the mixed layer, we observed two distinct sedimentation events. At first, sinking particles were dominated by small (diameter < 0.1 mm), slowly sinking (~ 18 m d^{-1}), particles rich in silica that carried a moderate POC flux (< 6 mmol C m^{-2} d^{-1}) to 500 m depth. Once the storms ceased, the volume of large (diameter > 0.1 mm), fast-sinking (> 75 m d^{-1}), carbon-rich marine snow aggregates (not fecal pellets) increased exponentially and POC fluxes at 100 m depth were more than fourfold greater (30 ± 12 mmol C m^{-2} d^{-1}) than those during the previous event. The aggregates consisted of a mixed post-bloom plankton community. Our data suggest that the storms shaped the timing, type, and magnitude of POC flux at the end of this spring phytoplankton bloom.

Spring phytoplankton blooms account for a significant fraction of the annual oceanic primary production and substantially contribute to carbon sequestration by the ocean (Henson et al. 2019; Siegel et al. 2023). The termination of a diatom bloom is frequently viewed as a single event of rapid diatom aggregation, triggered when nutrient limitation causes bloom senescence, and subsequent sedimentation of carbon-rich, fast-sinking diatom aggregates (sinking velocity > 50 m d^{-1}) (Alldredge and Silver 1988; Alldredge and Gotschalk 1989; Kiørboe et al. 1996). The result is the efficient export of particulate organic carbon (POC) to the ocean interior (Honjo et al. 1982; Smetacek 1985). The transition between bloom growth and export via marine snow is difficult to observe in the open ocean due to its ephemeral and spatially heterogeneous nature. We therefore lack a detailed understanding of the spatio-temporal dynamics of sinking particles during the declining phase of diatom blooms. However, such knowledge is key when predicting sinking particle flux and its carbon sequestration potential.

Marine snow aggregates form via coagulation of particles in the presence of high particle concentrations (e.g., phytoplankton and detritus) and increased levels of stickiness that enable attachment of particles that collide (Jackson 1990). Stickiness is provided by transparent exopolymer particles (TEP): gel-like particles largely composed of polysaccharides exuded as extracellular exopolymers (Passow 2002), especially under nutrient-limited conditions (Obernosterer and Herndl 1995). However, TEP are inherently positively buoyant (Engel and Schartau 1999; Azetsu-Scott and Passow 2004), and their role in regulating the sinking of particles is variable (Mari et al. 2017; Romanelli et al. 2023).

*Correspondence: elisa.romanelli@lifesci.ucsb.edu

Additional Supporting Information may be found in the online version of this article.

Author Contribution Statement: ER contributed to the design of the project, performed data acquisition and analysis, wrote, and revised the manuscript. SLG and ME, contributed to data acquisition, interpretation, and the writing of the manuscript. DAS and UP contributed to the design of the project, the interpretation of data, and the manuscript writing.

Another important factor controlling the formation of aggregates is the intensity of turbulent shear (Jackson 1990). Turbulence can enhance marine snow formation by promoting particle–particle collisions (Takeuchi et al. 2019). However, for higher dissipation rates (e.g., $> 10^{-6}$ W kg^{-1}), disaggregation may outcompete aggregation and hence limit marine snow size (Alldredge et al. 1990; Takeuchi et al. 2019). In the open ocean, turbulent kinetic energy dissipation rates in the mixed layer are mainly lower than 10^{-6} W kg^{-1} (Franks et al. 2022), with the higher rates occurring under intense storm conditions near the sea surface ($> 10^{-6}$ W kg^{-1}, Siegel et al. 2024). The impact of intense storms on sedimentation of marine snow aggregates has rarely been observed in situ (Siegel et al. 2024). However, storm severity is increasing due to climate change (e.g., Knutson et al. 2010), hence it is important to understand the impact of intense storms on marine particle dynamics.

Here we present detailed observations of marine particle dynamics immediately after the main sedimentation event of a spring diatom bloom (Brzezinski et al. 2024). This period was characterized by a series of intense storms that impacted sinking particle fluxes. To understand particle sedimentation under this post-bloom scenario, we characterized suspended, small sinking particles and fast-sinking marine snow collected using Marine Snow Catchers during the National Aeronautics and Space Administration (NASA)-led Export Processes in the Ocean from RemoTe Sensing (EXPORTS) North Atlantic field campaign (Johnson et al. 2024).

Methods

Characterization of the study site

Observations of particle characteristics were obtained in spring 2021 (May 4–29, 2021) on board the RRS James Cook, which targeted biogeochemical and ecological processes within an anticyclonic eddy in a Lagrangian manner (Johnson et al. 2024). The chosen eddy was long-lived and retentive as indicated by satellite altimetry and synthetic particle tracking analyses (Erickson et al. 2022). During the field campaign, four intense windstorms (hourly wind speeds exceeded 37 kt for each event) substantially deepened the mixed layer ($\Delta\rho$ threshold of $+0.05$ kg m^{-3}) by 25–40 m (Fig. 1a,b) and exchanged a variable, yet significant, fraction of the surface waters above the eddy's core with surrounding waters due to Ekman transport (Johnson et al. 2024). However, water parcels within 15 km from the eddy center and below a depth of ~ 100 m were retained throughout the cruise due to the eddy's low potential vorticity core (Erickson et al. 2022; Johnson et al. 2024). The Marine Snow Catchers were deployed in the retentive eddy core (at 8 ± 4 km from the eddy center).

To better investigate particle dynamics, we grouped the observations in five time periods (P) demarcated by the four

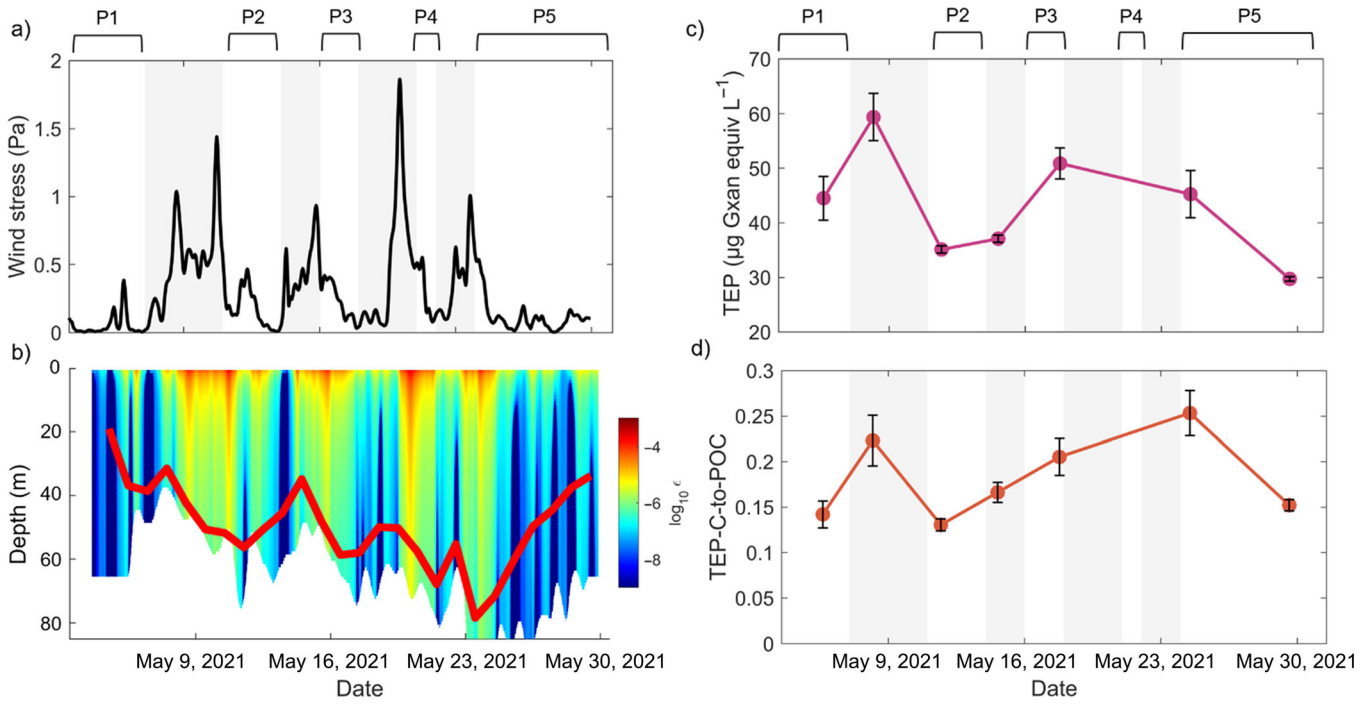

Fig. 1. Time series of (**a**) wind stress, (**b**) estimates of the turbulent kinetic energy dissipation rates in the mixed layer, and (**c**) concentrations of TEP, and (**d**) TEP-C-to-POC ratios measured in seawater collected with Niskin bottles within the mixed layer at ~ 20 m depth. Red line in (**b**) represents the depth of the daily mean mixed layer. Gray shading represents the storms. The five time periods demarcated by the storms (P1: May 4–7; P2: May 12–14; P3: May 16–19; P4: May 22; P5: May 25–29) are represented above (**a**) and (**c**). POC, particulate organic carbon; TEP, transparent exopolymer particles.

storms (P1: May 4–7; P2: May 12–14; P3: May 16–19; P4: May 22; P5: May 25–29; Fig. 1). The first storm (May 7–10) exchanged approximately 70–75% of the surface waters above the eddy core with surrounding waters (Johnson et al. 2024). Whereas for the subsequent storms, the estimated exchange of surface water in the eddy core (i.e., 15 km radius from center) was roughly 47%, 38% and 23%, respectively, (Johnson et al. 2024). Hence, observations collected during P2 through P5 are deemed as part of the same water parcel and have been interpreted as a time series.

Field sampling started at the end of a large diatom bloom as indicated by the extremely low silicate ($SiO_4 \sim 0.2\ \mu mol\ L^{-1}$) and relatively high nitrate ($NO_3 \sim 5\ \mu mol\ L^{-1}$) concentrations found in the mixed layer in P1 (Supporting Information Fig. S1). An analysis of the upper ocean silica budget showed that ~ 72% of the biogenic silica (bSi) produced during the diatom bloom had already been exported to depth (Brzezinski et al. 2024). Mixed layer concentrations of chlorophyll *a*, POC and bSi decreased significantly over time (Supporting Information Fig. S1) and vertically integrated rates of net primary production were reduced by > 50% by the end of the field sampling (Meyer et al. 2024; Supporting Information Fig. S1). The initial phytoplankton community in the mixed layer was dominated by diatoms; however, absolute and relative abundances of diatoms declined throughout the field campaign while the one of haptophytes and chlorophytes increased (Meyer et al. 2024).

Collection of suspended and sinking particles

Suspended and sinking particles were collected at 16 stations at 4 depth each, using four 100-liter Marine Snow Catchers (Lampitt et al. 1993). Deployments were performed in the morning (03:00–10:00 UTC, local time) except for two casts (on May 13 and May 25) conducted at 16:30 UTC. At each station, Marine Snow Catchers were deployed 10 and 100 m below the mixed layer, at either 300 or 500 m and at the deployment depths of the Neutrally Buoyant Sediment Traps (Estapa et al. 2024). Sampling and sample processing is detailed by Romanelli et al. (2023). Briefly, the Marine Snow Catcher is a 100-liter water sampler with a detachable top and base section that allows collecting particles according to their sinking velocity (Riley et al. 2012). To separately collect slow- and fast-sinking particles, a circular plastic tray (volume: ~ 1 liter) was placed at the bottom of the Marine Snow Catcher's base. This enabled three particle fractions to be separated according to their sampling location within the Marine Snow Catcher following 2 h of settling: *top* (*t*), *base* (*b*) and *tray* (*tr*). The *top* fraction, collected from the central tap, contained suspended particles. After draining and removing the top section, water overlying the tray in the base section was collected constituting the *base* particle fraction. The particle fraction in the tray was designated as the *tray* fraction. At nine stations, fast-sinking marine snow particles (equivalent spherical diameter [ESD] > 0.1 mm) were removed from the tray via manual pipetting, visually classified with a ruler (± 10%) into size bins of 0.5–1, 1–2, 2–4, and 4–8 mm (ESD) and preserved in 4% formaldehyde to perform microscopy later (Supporting Information Table S1). On May 27, fast-sinking marine snow was removed from the tray to measure its POC mass (Supporting Information Table S1). At three stations the entire particulate pool in the tray was processed as the *tray* fraction (i.e., marine snow was not removed) to enable estimates of the average sinking velocity of fast-sinking particles (Supporting Information Table S1). After removal of marine snow (Supporting Information Table S1; Fig. S2), the *top*, *base* and *tray* fractions were each mixed by shaking and subsampled for biochemical analysis. Mixed layer concentrations of POC and TEP (21 ± 5 m) were assessed at seven stations located within 15 km from the eddy center on samples collected with Niskin bottles mounted on a CTD-rosette.

Biochemical analysis

Concentrations of POC and particulate organic nitrogen (PON) were determined by filtering duplicate (triplicate for the Niskin samples) subsamples onto pre-combusted (450°C, 30 min) GF/F filters (25 mm, Whatman). We filtered 1 liter of the samples collected with the Niskin bottles, 1 liter of the MSC *top* fractions, 0.6–1 liters of the MSC *base* fraction and 0.2 liters of the MSC *tray* fraction. Filters were dried at 40°C and analyzed using a CEC 44OHA elemental analyzer (Control Equipment) after treatment with 150 μL of 10% HCl (v/v). The measured masses of POC and PON were blank-corrected to account for contamination using the cruise-wide EXPORTS' average (7.905 μg for POC; 1.782 μg for PON; $n = 26$) as in Graff et al. (2023). Values below the detection limit (29 of 423 PON) were removed. Negative values, which were within the standard deviation of replicates, were set to $0\ \mu g\ N\ L^{-1}$. The standard deviation of the replicates was 9–12% for POC and 24–32% for PON (Supporting Information Table S2). These values substituted for the uncertainty of measurements that lacked replicates (two POC and three PON).

Total particulate carbon was measured on one filter, like POC but without prior acidification. After subtraction of POC from particulate carbon, 39 out of 168 particulate inorganic carbon (PIC) values were negative and substituted with a $0\ \mu g\ PIC\ L^{-1}$.

Concentrations of bSi and lithogenic silica (lSi) were determined spectrophotometrically via the molybdosilicic acid method (Strickland and Parsons 1972; Tréguer et al. 1992). Filtered subsamples (47-mm PC filters, 0.6 μm, Isopore, Millipore) frozen at sea at −20°C and then dried at 60°C were digested in Teflon tubes by adding 4 mL of 0.2 N NaOH (95°C, 40 min), cooled immediately, neutralized by adding 1 mL of 1 M HCl, and centrifuged (10 min, 2500 rpm).

Concentrations of TEP were determined colorimetrically (Passow and Alldredge 1995). Triplicate subsamples of 400 mL were filtered (25-mm PC filters, 0.4-μm, Whatman), stained

with Alcian blue, and stored frozen. Samples and filter blanks were soaked for 2 h in 80% sulfuric acid (95% w/w; Fisher Scientific), and the absorption at 787 nm measured spectrophotometrically (Passow and Alldredge 1995). Xanthan gum (Sigma-Aldrich) was used to prepare standards (calibration *f*-factor was 34) and TEP expressed as xanthan gum equivalents (XGeq; Bittar et al. 2018). Absorbance values less than twice those of the blanks were considered below detection. The carbon concentration of TEP was estimated using a conversion factor of 0.75 μg TEP-C per 1 μg XGeq TEP (Engel and Passow 2001).

Calculations of particle concentrations

Particle concentrations were calculated from *top*, *base*, and *tray* concentrations:

$$\text{Suspended particles} = \textit{top}\ \text{concentration} \quad (1)$$

$$\text{Slow-sinking particles} = (\textit{base} - \textit{top}\ \text{concentrations}) \times V_{\text{base}}/V_{\text{MSC}} \quad (2)$$

$$\text{Fast-sinking particles} = (\textit{tray} - \textit{base}\ \text{concentrations}) \times V_{\text{tray}}/(A_{\text{tray}} \times h_{\text{MSC}}) \quad (3)$$

The volume of the base fraction ($V_{\text{base}} = 5.1$–6.1 liters) was calculated for each deployment as $V_{\text{base}} = V_{\text{bottom}} - (V_{\text{tray}}/0.466)$, where $V_{\text{MSC}} = 89.8$ liters, $V_{\text{bottom}} = 7.6$ liters, and the volume of seawater in the tray (V_{tray}) was 0.7–1.2 liters depending on deployment. The tray covers 46.6% of the area of the bottom of the MSC, hence we used 0.466 as scaling factor.

Removing fast-sinking marine snow particles from the tray allowed us to assess the concentration of small fast-sinking particles (ESD < 0.1 mm) separately from larger fast-sinking-marine snow. Marine snow was not observed in the *base* fraction; therefore, it can be assumed that on average slow-sinking particles were < 0.1 mm (ESD). Hence, for data interpretation, the concentrations of slow-sinking particles and the concentrations of small, fast-sinking particles (ESD < 0.1 mm) were summed into a single particle fraction termed "small sinking particles" (Supporting Information Table S3).

The concentration of fast-sinking marine snow in the water column was calculated by dividing the number of marine snow particles present in each tray by the associated V_{tray} and multiplied by the volume ratio ($V_{tray}/(A_{\text{tray}} \times h_{\text{MSC}})$). The volumetric concentration (ppmV) of fast-sinking marine snow was calculated assuming a sphere volume and an average diameter of 0.5, 1.5, 3, and 6 mm (midpoints of size bins: 0.1–1, 1–2, 2–4, and 4–8 mm).

POC concentrations associated with fast-sinking marine snow

We estimated the POC/N (μg) of fast-sinking marine snow collected on May 27 at 60 m (below the mixed layer depth, 30 m). Particulate organic carbon and PON was measured on 10–24 aggregates (ESD ~ 1 mm, ± 10%) per GF/F filter ($n = 8$), and POC and PON mass (μg) of individual marine snow was calculated after subtracting the POC and PON mass (μg) associated with 2.5 mL of tray water to account for contamination with smaller particles during pipetting. Since the dissolved organic carbon contained in their porewater (Alldredge 2000) was likely lost during filtration, the calculated values represent an underestimation of the organic carbon transported by marine snow. Five out of eight PON values were below detection. The average POC mass measured on 1-mm marine snow particles was 0.7 ± 0.1 μg agg^{-1} (Supporting Information Table S4), which is consistent with the one obtained using the fractal relationship of Alldredge (1998): POC (μg C) = 0.99 $V^{0.52}$ (V is volume in mm^3) for an aggregate with an ESD of 1 mm. We hence used this relationship to calculate the POC content of fast-sinking marine snow of different sizes, assuming a ± 25% uncertainty, which accounts for the standard deviation of the replicates (15%) and the error associated with the marine snow sizing (10%). Particulate organic carbon concentrations of marine snow were obtained by multiplying the POC mass by the concentration of marine snow in each size bin (method validation in Supporting Information).

The phytoplankton community composition associated with fast-sinking marine snow was visually and hence qualitatively assessed on the 4% formaldehyde-fixed samples collected on May 12, 17, 26, and 29 at 50–60 m depth using an Echo Revolve Microscope (Echo Laboratories) with a 10× objective.

Particle sinking velocity and POC fluxes

Particle fluxes were calculated by multiplying the concentration of sinking particles by an estimate of their average sinking velocity (Giering et al. 2016). The sinking velocity of slow-sinking particles collected with the Marine Snow Catcher is on average 18 m d^{-1} based on its dimensions (Giering et al. 2016), and the sinking velocity of fast-sinking particles is greater than 18 m d^{-1}. To constrain the sinking velocity of fast-sinking particles (sum of small, fast-sinking particles and fast-sinking marine snow), we compared simultaneous deployments of Marine Snow Catchers and drifting sediment traps assuming that sediment traps collect both slow- and fast-sinking particles, and that the sinking velocity of slow-sinking particles is known. Three times (May 12, 17, and 25), Marine Snow Catchers were deployed at the same depths as the drifting traps ((a) 73 and 174 m, (b) 175 m, and (c) 95, 145, 195, and 500 m, respectively). Surface-tethered and neutrally buoyant sediment traps deployment and methodology used to assess bulk POC fluxes is described in Estapa et al. (2024). To calculate the average sinking velocity of fast-sinking particles, we first calculated the POC flux due to fast-sinking particles measured by traps by subtracting the Marine Snow Catchers slow-sinking POC fluxes from the trap POC fluxes. The sinking velocities of fast-sinking particles are then

the trap fast-sinking POC fluxes divided by the POC concentrations of fast-sinking particles from the Marine Snow Catcher. Fast-sinking POC fluxes from the Marine Snow Catchers are the product of the sinking velocity and the fast-sinking POC concentrations. The error associated with each sinking velocity and POC flux was calculated by propagating the standard deviation of the individual measurements through each calculation. As the sinking velocity of fast-sinking particles was assessed only on 3 days and at a few depths, we averaged the sinking velocities to be able to calculate the POC fluxes of particles collected in between such values (Supporting Information Table S5). Traps may partially underestimate small particles due to hydrodynamics (Buesseler et al. 2007), therefore our sinking velocity and POC fluxes should be considered a lower bound.

Turbulent kinetic energy dissipation rates

Estimates of turbulent kinetic energy dissipation rates (ϵ, W kg^{-1}) were derived from established scaling relationships (Lombardo and Gregg 1989; D'Asaro et al. 2014) using air–sea momentum and buoyancy flux determinations calculated from bulk formulae (Johnson et al. 2024). These scaling estimates of ϵ are valid in the near-surface mixed layer (Siegel et al. 2024).

Statistical analyses

Simple linear regression was used to test (significance threshold of 0.05) for statistically significant temporal trends displayed by particle and biochemical concentrations. The assumption of normal distribution for the linear regressions were assessed visually (qq-plots) and statistically using the Shapiro–Wilk test ($p > 0.05$). The linear analyses were performed using the function fitlm in Matlab (R2023a). Data can be found at NASA SeaBASS data repository.

Results

Variable turbulence levels in the mixed layer

The four storms (Fig. 1a) created intense turbulence in the mixed layer where turbulent kinetic energy dissipation rates varied in time by several orders of magnitude (Fig. 1b; Siegel et al. 2024). The five time periods (P1–P5) were characterized by moderate turbulent kinetic energy dissipation rates of $< 10^{-6}$ W kg^{-1} and were separated by the intense storm events with near-surface turbulent kinetic energy dissipation rates $> 10^{-4}$ W kg^{-1}.

Concentrations of POC and TEP in the mixed layer

Concentrations of POC measured at ~ 20 m depth within the mixed layer decreased from 17 ± 2 μmol C L^{-1} to 12 ± 1 μmol C L^{-1} ($n = 6$, $\pm$ variability among replicates) between P2 and P5 (Supporting Information Fig. S1). The corresponding concentrations of TEP (Fig. 1c) increased from 35 μg XGeq L^{-1} in P2 (May 11) to 51 μg XGeq L^{-1} in P3 (May 17), remained constant in P3–P4, and decreased to 30 μg XGeq L^{-1} by the end of P5 (May 29). Concurrently, the relative contribution of TEP-C to POC (TEP-C-to-POC ratios) increased from 0.13 in P2 (May 11) to 0.25 at the beginning of P5 (May 24) (Fig. 1d). The steepest decline in TEP and TEP-C-to-POC ratios occurred during P5.

Characteristics of suspended particles

The POC concentrations of suspended particles collected with the Marine Snow Catchers were highest below the mixed layer at 50–75 m after the first two storms (May 13, 10 μmol C L^{-1}, and May 17, 9.3 μmol C L^{-1}; Fig. 2a). Thereafter, suspended POC concentrations decreased significantly in that depth range (May 17–29; $R^2 = 0.55$, $p = 0.02$, $n = 8$). Yet, they remained constant at 90–140, 330, and 500 depth ($R^2 \leq 0.30$, $p \geq 0.21$, $n = 10$, 3, and 5, respectively) (Fig. 2a). The PON and bSi concentrations of suspended particles broadly mirrored the spatiotemporal trend of suspended POC (Supporting Information Fig. S3a,b). However, the ratio between bSi and POC changed appreciably (Fig. 2b). The molar bSi-to-POC ratio of suspended particles was the highest in P3 and decreased significantly from P3 to P5 at 50–75, 90–140, and 330 m ($R^2 \geq 0.48$, $p < 0.04$, $n = 6$, 8, and 3, respectively). No significant temporal trend in the molar bSi-to-POC ratio of suspended particles was observed at 500 m depth ($R^2 = 0.36$, $p = 0.28$, $n = 5$).

Characteristics of small sinking particles

The POC concentration of small sinking particles peaked at 50–75 m in P3 (May 17) (0.95 μmol C L^{-1}) and decreased significantly in P3–P5 ($R^2 = 0.92$, $p < 0.007$, $n = 5$; Fig. 2c). The POC concentrations of small sinking particles did not show a significant change over time below the 50–75 m depth layer ($R^2 \leq 0.29$, $p \geq 0.21$, $n = 10$, 4, and 7 at 90–140, 330, and 500 m, respectively). The concentration of PON in small sinking particles mirrored the evolution of POC (Supporting Information Fig. S3c).

The bSi concentration of small sinking particles at 50–75 m was the highest in P3 (May 17) and at the beginning of P5 (May 26). At 90–330 m depth, bSi concentrations increased from P2 to P3, whereas at 500 m, a significant increase was observed from the end of P3–P5 ($R^2 = 1$, $p < 0.001$, $n = 3$) (Supporting Information Fig. S3d).

The molar ratios of bSi-to-POC of small sinking particles at 50–75 m depth doubled from P3 to the beginning of P5 (May 26) and halved within P5 from May 26 to 29 (Fig. 2d). At 90–140 and 500 m depth, the bSi-POC ratios increased from P2 to P5 ($R^2 = 0.66$, $p < 0.003$, $n = 10$ and $R^2 = 0.67$, $p = 0.058$, $n = 5$, respectively).

Molar PIC-to-POC ratios in small sinking particles did not show any significant evolution over time ($R^2 \leq 0.43$, $p = \leq 0.77$, $n = 8$, 8, 4, and 5 at 50–75, 90–140, 330, and 500 m, respectively) (Supporting Information Fig. S3e). Similarly, molar POC-to-PON ratios did not show any trend over time or depth. However, molar lithogenic silica to POC ratios of small sinking particles ($n = 3$) showed a sharp decrease over

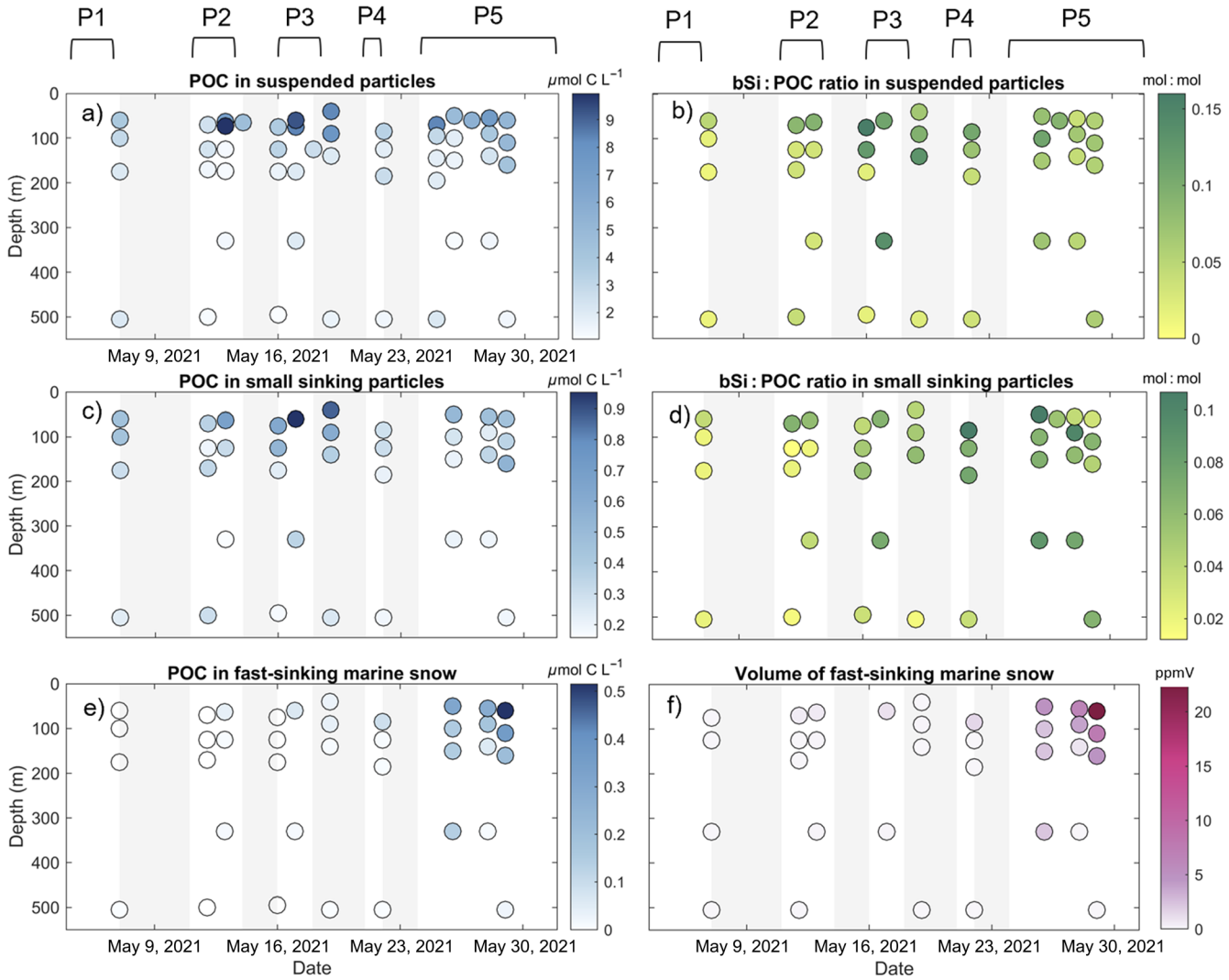

Fig. 2. Time-depth distributions of particle characteristics for (**a**, **b**) suspended particles, (**c**, **d**) small sinking particles and (**e**, **f**) fast-sinking marine snow. Left panels show POC concentrations (**a**, **c**, **e**). Right panels show molar bSi-to-POC ratios for suspended and small sinking particles (**b**, **d**) and, volumetric concentrations of fast-sinking marine snow particles (**f**). The five time periods (P) demarcated by the storms (P1: May 4–7; P2: May 12–14; P3: May 16–19; P4: May 22; P5: May 25–29) are represented above (**a**) and (**b**). Gray shading represents the storms. bSi, biogenic silica; POC, particulate organic carbon.

time due to the complete disappearance of lithogenic silica in small sinking particles at the end of P5 (May 28) (Supporting Information Fig. S3f).

Taken together (Fig. 2b,d) the spatiotemporal changes of bSi : POC in suspended and small sinking particles suggest sinking of small particles rich in silica, which in the discussion, we refer to as the first sedimentation event (P2–P4).

Characteristics of fast-sinking marine snow

The volumetric concentration (ppmV) of fast-sinking marine snow increased exponentially from P2 to P5 ($R^2 = 0.95$–0.99, $n = 7$, 8, and 5 at 50–75, 90–125, and 500 m, respectively) with P5 characterized by the highest volume concentrations (Fig. 2f). Similarly, the POC concentrations of fast-sinking marine snow increased significantly over time from P2 to P5 ($R^2 = 0.79$, $p < 0.03$, $n = 5$ at 50–63 m and $R^2 = 0.29$, $p < 0.03$, $n = 7$ at 90–125 m) and were highest at the end of P5 (May 29), when they were 0.52 and 0.02 μmol C L^{-1} at 60 and 500 m, respectively (Fig. 2e). In the discussion we refer to the sinking of fast-sinking marine snow aggregates as the second sedimentation event.

The plankton community composition associated with fast-sinking marine snow collected at 50–75 m transitioned during the field campaign. We observed the presence of detrital diatoms initially and an increased contribution of heterotrophs and healthy diatoms by the end of P5 (Supporting Information Fig. S4). Specifically, in P2 (May 12), marine snow contained mostly detrital diatoms (empty and broken frustules) mainly *Chaetoceros* spp. and Navicula-type pennates,

but also *Rhizosolenia* spp., silicoflagellates (haptophytes), and Tintinnids (heterotrophic ciliates). In P3 (May 17), we observed an increase in the relative abundance of dinoflagellates, including autotrophs (*Ceratium* spp.) and hetero- or mixotrophic taxa, whereas the relative abundance of silicoflagellates and *Chaetoceros* spp. appeared to decrease compared to P2. At the beginning of P5 (May 26), marine snow composition was similar to the one observed in P3 with the addition of radiolarians. On the last day of P5 (May 29), marine snow did not contain silicoflagellates and was likely largely composed of heterotrophs (dinoflagellates, tintinnids), although intact diatoms also increased (Supporting Information Fig. S4).

Sinking velocity of fast-sinking particles

The sinking velocity of fast-sinking particles (small fast-sinking particles plus fast-sinking marine snow) above 200 m depth was on average 52 ± 46 m d^{-1} ($n = 9$) and increased over time from an average (± variability among estimates) of 17 ± 5 m d^{-1} ($n = 5$) in P2–P3 to an average of 97 ± 30 m d^{-1} ($n = 4$) in P5 (Fig. 3; Supporting Information Table S5). This increase was concurrent with the increase in the volumetric concentration of fast-sinking marine snow observed in P5 (Fig. 2f). From P2 to P5, the average contribution of small sinking particles (slow-sinking particles plus small, fast-sinking particles) to the total POC concentration of sinking particles decreased from 99% to 54%. The sinking velocities estimated in P2–P3 were therefore almost fully representative of the sinking velocity of small sinking particles, whereas the sinking velocity in P5 includes the contribution of fast-sinking marine snow. In P2–P3, when marine snow was rare, fast-sinking particles sank at approximately the same velocity as slow-sinking particles (18 m d^{-1}). At the beginning of P5 at 500 m depth, the sinking velocity of fast-sinking particles was 42 ± 5 m d^{-1} (Fig. 3).

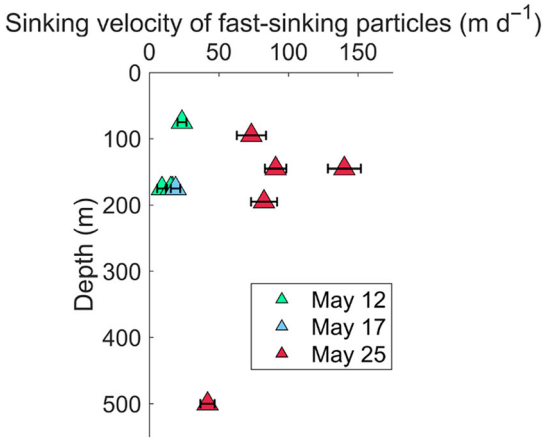

Fig. 3. Temporal and vertical variations in the estimated sinking velocities of fast-sinking particles (small, fast-sinking particles plus fast-sinking marine snow) calculated from a comparison of Marine Snow Catchers collections and bulk sediment trap POC fluxes. Error bars are the propagated measurement standard deviations. POC, particulate organic carbon.

Sinking particle POC fluxes

The POC flux of the total sinking particle pool (slow-sinking plus fast-sinking particles) peaked after the fourth storm at the end of P5 (May 29). Particulate organic carbon fluxes increased significantly over time from P2 to P5 at the depths 50–75 and 90–140 m ($R^2 = 0.65$–0.8, $p < 0.001$, $n = 12$ and 14, respectively) but did not at 500 m ($R^2 = 0.36$, $p = 0.15$, $n = 7$) (Fig. 4a). Specifically, at 90–125 m fluxes were 6 ± 3 mmol C m^{-2} d^{-1} ($n = 8$) in P2–P4 and a factor of 4.7 higher (30 ± 12 mmol C m^{-2} d^{-1}) in P5 ($n = 6$). The contribution of fast-sinking particles to the total POC flux (slow-sinking plus fast-sinking particles) was highest (95% of the total) during P5 between 50 and 70 m depth. At 50–75 and 90–125 m depth, this contribution increased significantly from P2 to P5 (between May 13 and May 29; $R^2 \geq 0.67$, $p < 0.003$, $n = 12$ and 12, respectively; Fig. 4b). No significant temporal trend was observed at 500 m ($R^2 = 0.004$, $p = 0.90$, $n = 6$).

Discussion

We observed two sedimentation events during our field campaign, both after the main diatom sedimentation event that occurred prior to our ship-based observations (Fig. 5). The first sedimentation event (from P2 to P4) was dominated by

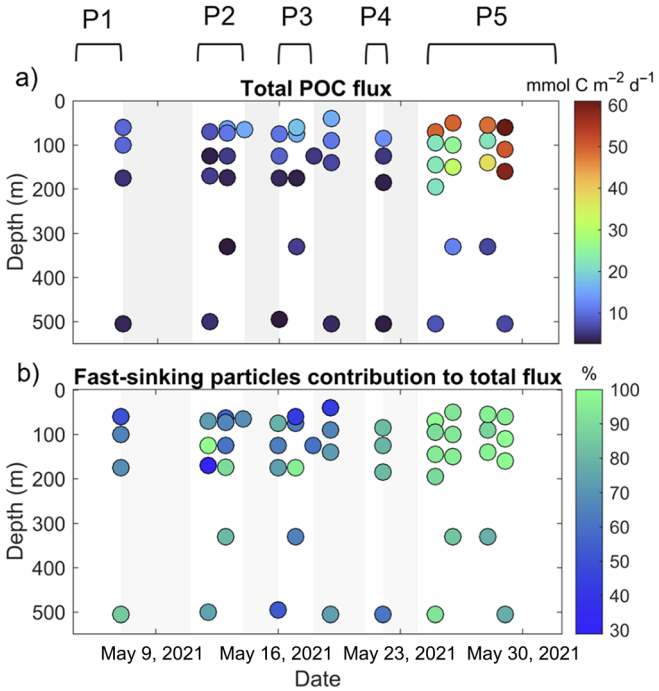

Fig. 4. Time–depth distributions of (**a**) total POC flux (due to both slow-sinking and fast-sinking particles) and (**b**) fractional (%) contribution of POC flux due to fast-sinking particles to total POC flux. POC, particulate organic carbon.

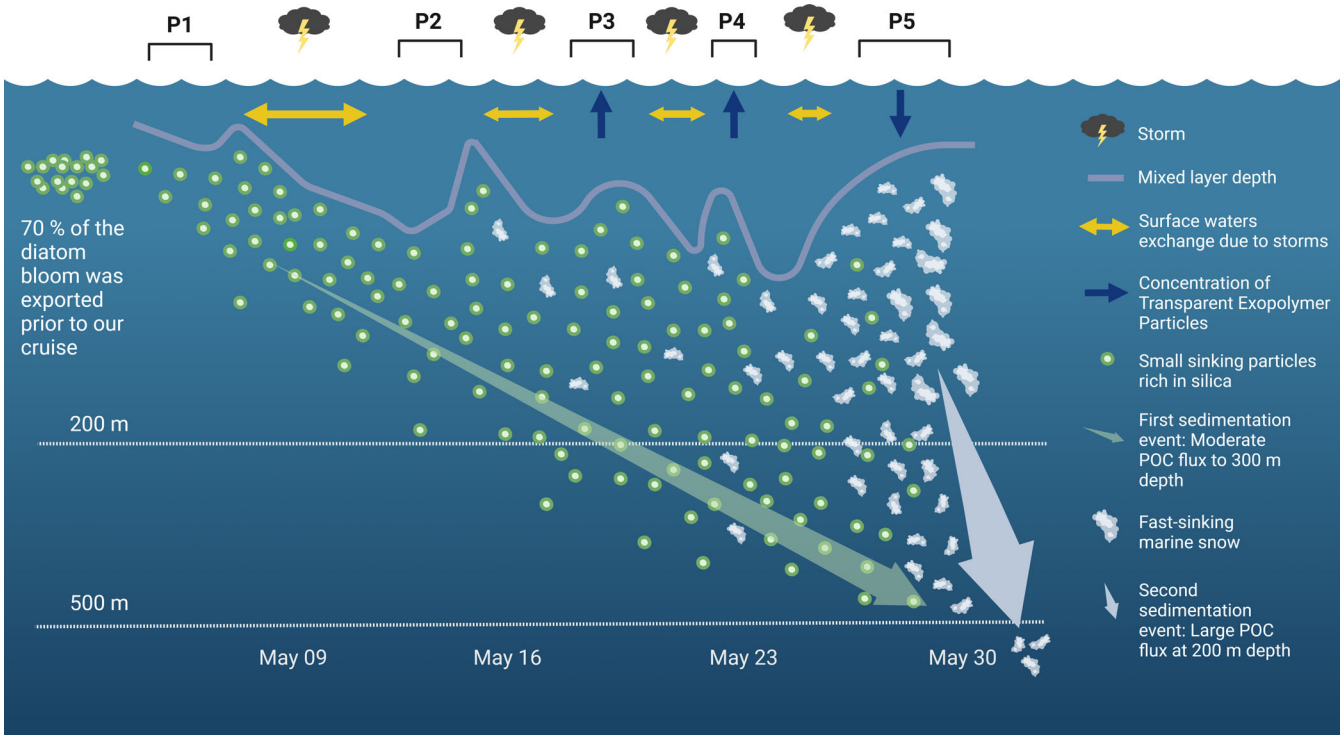

Fig. 5. Schematic of the two sedimentation events that followed the main diatom export prior to our arrival on this site. P2–P4: First sedimentation event (transparent green arrow): Small sinking particles rich in silica sank in the upper mesopelagic. The storm events exchanged decreasing fractions of surface waters. Concurrently, TEP accumulated in the mixed layer (as indicated by the upward blue arrows) while the volume concentration of fast-sinking marine snow remained low. These small sinking particles created a moderate POC flux at 300 m depth. P5: Second sedimentation event (transparent white arrow): The volume concentration of fast-sinking marine snow increased exponentially at the beginning of P5 when the storms ceased, turbulence was moderately intense, and the mixed layer depth shallowed to approximately 30 m depth. The TEP concentrations within the mixed layer decreased. This second sedimentation event displayed the potential for substantial and efficient POC export to below 500 m depth. POC, particulate organic carbon; TEP, transparent exopolymer particles.

small sinking particles rich in silica (Figs. 2 and 5). The second sedimentation event (predominantly observed during P5 but starting late P4) consisted of fast-sinking marine snow aggregates, which increased after the series of storms ceased (Fig. 5). Our data suggest that the two sedimentation events partially overlapped. During P4, 24% of the POC concentration measured in sinking particles was due to fast-sinking marine snow at 85 m depth; however, between 125 and 500 m depth, small sinking particles were still dominating flux (99% of POC in sinking particles). By the beginning of P5 (May 25) the contribution of fast-sinking marine snow increased to 39% at all depths to 330 m.

In the following sections, we characterize mechanisms driving each sedimentation event and discuss their respective potential contributions to vertical POC transport in the upper mesopelagic.

First sedimentation event: Moderate POC fluxes due to small sinking particles during P2–P4

Our data, particularly the molar bSi-to-POC ratios, indicate the flux of small sinking particles rich in silica below the mixed layer down to 300 m during the time periods P2–P4. This observation is consistent with the increased flux of intact, empty, and broken diatoms measured in polyacrylamide gel sediment traps between P2 and P4 (Bodel 2023).

During each storm, the mixed layer deepened, mixing particles to depth, where particles would subsequently be isolated from the surface as the mixed layer shallowed (10–30 m below the mixed layer, Siegel et al. 2024). This process transported particles to depth in a process similar to the mixed layer pump (Gardner et al. 1995; Dall'Olmo and Mork 2014; Giering et al. 2016). An assessment of the upper ocean silica budget performed by Brzezinski et al. (2024) showed that the bSi isolated below the mixed layer between storms accounts for most of the bSi exported during P1–P3. Once below the mixed layer, in more quiescent waters, small sinking particles rich in silica were able to settle gravitationally. Some of these particles grew in size due to shear aggregation (Siegel et al. 2024) and thereby sunk further. The bulk sinking velocity of these small sinking particles as estimated from the Marine Snow Catcher was low ($\sim$ 18 m d^{-1}, Fig. 3) compared to large marine snow, but much faster than commonly expected for small detrital particles (Bach et al. 2012), likely due to the high silica content.

Because of their relatively low sinking velocity, the POC in small sinking particles was likely mostly recycled through the food web in the shallow mesopelagic zone rather than transported to or below 500 m. Shallow remineralization is supported by the lack of an increase in the POC concentrations of small sinking particles at and below 200 m depth (Fig. 2c). Flux profiles estimated from the Thorium-234 disequilibrium method show a decrease of POC fluxes between the mixed layer and 100 m depth and a concurrent increase of bSi fluxes during P2–P4 (Clevenger et al. 2024), supporting the idea of shallow POC remineralization.

Second sedimentation event: High POC fluxes due to fast-sinking marine snow after the storms

The rapid sedimentation of fast-sinking marine snow aggregates mainly developed after the last storm ceased, more than 3 weeks after the main sedimentation event of the bloom. The formation of marine snow aggregates requires the presence of TEP, which promotes adhesion after collision (Logan et al. 1995). During P2–P4, we observed an accumulation of TEP in the mixed layer (Fig. 1d). Enhanced TEP production has been linked to diatoms during the termination phase of their blooms (Passow and Alldredge 1995).

The subsequently observed decrease in concentrations of mixed layer TEP in P5 is consistent with TEP removal as part of flux of marine snow particles to depth.

The combination of diatoms, increased mixed layer TEP concentrations and turbulence (Figs. 1, 2) observed in P2–P4 could have resulted in the formation and subsequent sinking of large marine snow aggregates. However, large marine snow (> 0.1 mm) aggregates mainly formed at the end of the series of storms, after P4. The high turbulent kinetic energy dissipation rates created by the storms (Fig. 1) led to turbulent shear disaggregation creating small particles from larger particles (Siegel et al. 2024). This disaggregation process is supported by a strong reduction in the volumes of large particles (diameter between ~ 0.5 and 5 mm) obtained from in situ imaging of particles in the mixed layer during P2–P4 (Siegel et al. 2024). After each storm, when mixed layer turbulent levels decreased (Fig. 1), particle sizes and volumes rapidly increased, again likely due to shear coagulation, with peak particle sizes occurring at intermediate turbulence levels (Siegel et al. 2024). These conclusions are in line with experimental evidence that high turbulence levels, above $\sim 10^{-6}$ W kg^{-1}, leads to fragmentation and destruction of large marine snow in the mixed layer (Alldredge et al. 1990; Takeuchi et al. 2019). We thus postulate that the high levels of turbulence during the storms prevented the formation of large marine snow aggregates. Net marine snow formation was observed as soon as the storm events ended after during P5 (Fig. 2f, Siegel et al. 2024). This change in aggregation dynamics likely explains the net appearance of large marine snow after the series of storms had passed and when turbulence levels in the mixed layer promoted higher aggregation rates. In addition, the deepening of the mixed layer during the storms and its restratification thereafter, created a layer of high particle concentrations just below the mixed layer at moderate turbulence, which likely also allowed the formation of large marine snow as shown by Siegel et al. 2024. We observed high concentrations of marine snow down to 350 m depth during P5, probably including both sinking marine snow formed in the mixed layer after the storms and sinking marine snow formed below the mixed layer from particles isolated there when the mixed layer shallowed again after the last storm.

Not only did the volumetric concentration of marine snow aggregates increased dramatically during P5, but the composition of the fast-sinking marine snow aggregates also changed over time, shifting from detrital diatoms (P2) to marine snow that reflected a community of intact diatoms and heterotrophic taxa (specifically, dinoflagellates and tintinnids) (P5) (Supporting Information Fig. S4). Detrital diatoms at the beginning of our study are in line with the end phase of a main diatom bloom sedimentation event. The intact diatoms observed towards the end of our study (P5) in sinking marine snow may have originated from growing diatoms that were using the silicic acid injected by the mixed layer entrainment caused by the storms (Brzezinski et al. 2024; Johnson et al. 2024), as diatoms are able to recover from silica limitation within hours (De La Rocha and Passow 2004). High abundances of dinoflagellates and tintinnids were also seen in the marine snow aggregates and their presence has previously been observed at the end of diatom blooms (Passow and Peinert 1993; Tiselius and Kuylenstierna 1996; Sherr and Sherr 2007).

Our data also indicate that the fast-sinking marine snow in P5 created a large POC flux. The calculated POC fluxes at 100 m depth (51 ± 15 mmol C m^{-2} d^{-1}, May 29) are on the high end of observed upper ocean POC fluxes (Mouw et al. 2016; Bisson et al. 2020; Giering et al. 2023). In addition, our data suggest that this POC flux had the potential to rapidly reach the depth of the winter mixed layer (600 m in the North Atlantic, de Boyer Montégut et al. 2004) and hence to be sequestered for a relevant amount of time. This statement is supported by the large carbon content (0.7 μg C agg^{-1}) of the marine snow aggregates and the high average sinking velocities of fast-sinking particles (97 ± 30 m d^{-1}, $n = 4$). This measured average sinking velocity represents an average of the entire fast-sinking particle population, including particles smaller than 0.1 mm in diameter. Hence the large marine snow aggregates that we observed were likely sinking faster than this estimate of average sinking. In addition, this sinking velocity, which was measured at the beginning of P5 (May 25) is likely an underestimation of the sinking velocity of the fast-sinking particles presents in the water at the end of P5 (May 29). In fact, the volumetric concentration of fast-sinking marine snow at 60 m depth increased by 3.5-fold during P5 increasing the proportion of large marine snow in the fast-sinking particle pool.

Conclusion

We present observations of suspended and sinking particles and their sinking fluxes in the decline of the North Atlantic spring bloom and their transformations due to a series of intense storms. Giering et al. (2016) found a two orders-of-magnitude increase in the concentration of large particles above 100 m depth after a strong spring storm (9–10 on the Beaufort wind force scale) in the high latitudes of the North Atlantic. We here show data that provide a detailed characterization of particle dynamics and fluxes under similarly strong storm conditions. First, destabilization of the water column during storms (shear disaggregation and mixed layer pump) may allow the transport of small sinking particles into the upper mesopelagic. Second, the delay in the formation of large, fast-sinking marine snow due to storms, may result in carbon flux to below the deep winter mixed layer that includes carbon stemming from a transitioning, mixed plankton community. Including such significant "non-spring bloom" sedimentation events in our assessment of the biological carbon pump will improve model predictions of flux and evaluations of the consequences of marine carbon dioxide removal technologies.

Data availability statement

All data presented here are publicly available on the NASA data repository, SeaBASS along with all other EXPORTS data. The data can be accessed at https://seabass.gsfc.nasa.gov/experiment/EXPORTS.

References

Alldredge, A. 1998. The carbon, nitrogen and mass content of marine snow as a function of aggregate size. Deep-Sea Res. I Oceanogr. Res. Pap. **45**: 529–541.

Alldredge, A. L. 2000. Interstitial dissolved organic carbon (DOC) concentrations within sinking marine aggregates and their potential contribution to carbon flux. Limnol. Oceanogr. **45**: 1245–1253.

Alldredge, A. L., and M. W. Silver. 1988. Characteristics, dynamics and significance of marine snow. Prog. Oceanogr. **20**: 41–82.

Alldredge, A. L., and C. C. Gotschalk. 1989. Direct observations of the mass flocculation of diatom blooms: Characteristics, settling velocities and formation of diatom aggregates. Deep-Sea Res. A. Oceanogr. Res. Pap. **36**: 159–171.

Alldredge, A. L., T. C. Granata, C. C. Gotschalk, and T. D. Dickey. 1990. The physical strength of marine snow and its implications for particle disaggregation in the ocean. Limnol. Oceanogr. **35**: 1415–1428.

Azetsu-Scott, K., and U. Passow. 2004. Ascending marine particles: Significance of transparent exopolymer particles (TEP) in the upper ocean. Limnol. Oceanogr. **49**: 741–748.

Bach, L. T., U. Riebesell, S. Sett, S. Febiri, P. Rzepka, and K. G. Schulz. 2012. An approach for particle sinking velocity measurements in the 3–400 μm size range and considerations on the effect of temperature on sinking rates. Mar. Biol. **159**: 1853–1864.

Bisson, K., D. A. Siegel, and T. DeVries. 2020. Diagnosing mechanisms of ocean carbon export in a satellite-based food web model. Front. Mar. Sci. **7**: 505.

Bittar, T. B., U. Passow, L. Hamaraty, K. D. Bidle, and E. L. Harvey. 2018. An updated method for the calibration of transparent exopolymer particle measurements. Limnol. Oceanogr.: Methods **16**: 621–628.

Bodel, A. 2023. The solitary sinking phytoplankton cell and the biological carbon pump. Capstone projects and Master's theses. Moss Landing Marine Laboratories.

Brzezinski, M. A., L. Johnson, M. Estapa, S. Clevenger, M. Roca-Martí, E. Romanelli, K. N. Buck, B. D. Jenkins, and J. L. Jones. 2024. Physical mechanisms sustaining silica production following the demise of the diatom phase of the North Atlantic spring phytoplankton bloom during EXPORTS. Global Biogeochem. Cycl. **38**: e2023GB008048.

Buesseler, K. O., and others. 2007. An assessment of the use of sediment traps for estimating upper ocean particle fluxes. J. Mar. Res. **65**: 345–416.

Clevenger, S. J., C.R. Benitez-Nelson, M. Roca-Martí, W. Bam, M. Estapa, J. A. Kenyon, S. Pike, L. Resplandy, A. Wyatt, and K. O. Buesseler. 2024. Carbon and silica fluxes during a declining North Atlantic spring bloom as part of the EXPORTS program. Mar Chem. **258**: 104346.

Dall'Olmo, G., and K. A. Mork. 2014. Carbon export by small particles in the Norwegian Sea. Geophys. Res. Lett. **41**: 2921–2927. doi:10.1002/2014GL059244

D'Asaro, E. A., J. Thomson, A. Y. Shcherbina, R. R. Harcourt, M. F. Cronin, M. A. Hemer, and B. Fox-Kemper. 2014. Quantifying upper ocean turbulence driven by surface waves. Geophys. Res. Lett. **41**: 102–107.

de Boyer Montégut, C., G. Madec, A. S. Fischer, A. Lazar, and D. Iudicone. 2004. Mixed layer depth over the global ocean: An examination of profile data and a profile-based climatology. J. Geophys. Res. Oceans **109**.

De La Rocha, C. L., and U. Passow. 2004. Recovery of *Thalassiosira weissflogii* from nitrogen and silicon starvation. Limnol. Oceanogr. **49**: 245–255.

Engel, A., and M. Schartau. 1999. Influence of transparent exopolymer particles (TEP) on sinking velocity of *Nitzschia closterium* aggregates. Mar. Ecol. Prog. Ser. **182**: 69–76.

Engel, A., and U. Passow. 2001. Carbon and nitrogen content of transparent exopolymer particles (TEP) in relation to their Alcian Blue adsorption. Mar. Ecol. Prog. Ser. **219**: 1–10.

Erickson, Z. K., and others. 2022. EXPORTS North Atlantic eddy tracking. NASA Technical Memorandum. doi:10.1575/1912/29464

Estapa, M. L., C. A. Durkin, W. H. Slade, C. L. Huffard, S. P. O'Neill, and M. M. Omand. 2024. A new, global optical sediment trap calibration. Limnol. Oceanogr.: Methods. **22**: 77–92.

Franks, P. J., B. G. Inman, J. A. MacKinnon, M. H. Alford, and A. F. Waterhouse. 2022. Oceanic turbulence from a planktonic perspective. Limnol. Oceanogr. **67**: 348–363.

Gardner, W. D., S. P. Chung, M. J. Richardson, and I. D. Walsh. 1995. The oceanic mixed-layer pump. Deep-Sea Res. II Top. Stud. Oceanogr. **42**: 757–775.

Giering, S. L. C., R. Sanders, A. P. Martin, C. Lindemann, K. O. Möller, C. J. Daniels, D. J. Mayor, and M. A. St. John. 2016. High export via small particles before the onset of the North Atlantic spring bloom. J. Geophys. Res. Oceans **121**: 6929–6945.

Giering, S. L. C., and others. 2023. Vertical imbalance in organic carbon budgets is indicative of a missing vertical transfer during a phytoplankton bloom near South Georgia (COMICS). Deep-Sea Res. II Top. Stud. Oceanogr. **209**: 105277.

Graff, J. R., and others. 2023. Reconciliation of total particulate organic carbon and nitrogen measurements determined using contrasting methods in the North Pacific Ocean as part of the NASA EXPORTS field campaign. Element. Sci. Anthrop. **11**.

Henson, S., F. Le Moigne, and S. Giering. 2019. Drivers of carbon export efficiency in the global ocean. Global Biogeochem. Cycl. **33**: 891–903.

Honjo, S., S. J. Manganini, and J. J. Cole. 1982. Sedimentation of biogenic matter in the deep ocean. Deep-Sea Res. A. Oceanogr. Res. Pap. **29**: 609–625.

Jackson, G. A. 1990. A model of the formation of marine algal flocs by physical coagulation processes. Deep-Sea Res. A Oceanogr. Res. Pap. **37**: 1197–1211.

Johnson, L., and others. 2024. Assessment of oceanographic conditions during the North Atlantic EXport processes in the ocean from RemoTe Sensing (EXPORTS) field campaign. Prog. Oceanogr. **103170**: 103170. doi:10.1016/j.pocean.2023.103170

Kiørboe, T., J. L. Hansen, A. L. Alldredge, G. A. Jackson, U. Passow, H. G. Dam, D. T. Drapeau, A. Waite, and C. M. Garcia. 1996. Sedimentation of phytoplankton during a diatom bloom: Rates and mechanisms. J. Mar. Res. **54**: 1123–1148.

Knutson, T. R., and others. 2010. Tropical cyclones and climate change. Nat. Geosci. **3**: 157–163.

Lampitt, R. S., K. F. Wishner, C. M. Turley, and M. V. Angel. 1993. Marine snow studies in the Northeast Atlantic Ocean: Distribution, composition and role as a food source for migrating plankton. Mar. Biol. **116**: 689–702.

Logan, B. E., U. Passow, A. L. Alldredge, H. P. Grossartt, and M. Simont. 1995. Rapid formation and sedimentation of large aggregates is predictable from coagulation rates (half-lives) of transparent exopolymer particles (TEP). Deep-Sea Res. II Top. Stud. Oceanogr. **42**: 203–214.

Lombardo, C. P., and M. C. Gregg. 1989. Similarity scaling of viscous and thermal dissipation in a convecting surface boundary layer. J. Geophys. Res. Oceans **94**: 6273–6284.

Mari, X., U. Passow, C. Migon, A. B. Burd, and L. Legendre. 2017. Transparent exopolymer particles: Effects on carbon cycling in the ocean. Prog. Oceanogr. **151**: 13–37.

Meyer, M. G., M. A. Brzezinski, M. R. Cohn, S. J. Kramer, N. Paul, G. Sharpe, A. K. Niebergall, S. Gifford, N. Cassar, and A. Marchetti. 2024. Size-fractionated primary production dynamics during the decline phase of the North Atlantic spring bloom. Global Biogeochem Cy. **38** e2023GB008019.

Mouw, C. B., A. Barnett, G. A. McKinley, L. Gloege, and D. Pilcher. 2016. Global ocean particulate organic carbon flux merged with satellite parameters. Earth Syst. Sci. Data **8**: 531–541.

Obernosterer, I., and G. J. Herndl. 1995. Phytoplankton extracellular release and bacterial growth: Dependence on the inorganic N:P ratio. Mar. Ecol. Prog. Ser. **116**: 247–257.

Passow, U. 2002. Transparent exopolymer particles (TEP) in aquatic environments. Prog. Oceanogr. **55**: 287–333.

Passow, U., and R. Peinert. 1993. The role of plankton in particle flux: Two case studies from the northeast Atlantic. Deep-Sea Res. II Top. Stud. Oceanogr. **40**: 573–585.

Passow, U., and A. L. Alldredge. 1995. A dye-binding assay for the spectrophotometric measurement of transparent exopolymer particles (TEP). Limnol. Oceanogr. **40**: 1326–1335.

Riley, J. S., R. Sanders, C. Marsay, F. A. Le Moigne, E. P. Achterberg, and A. J. Poulton. 2012. The relative contribution of fast and slow sinking particles to ocean carbon export. Global Biogeochem. Cycles **26**.

Romanelli, E., J. Sweet, S. L. C. Giering, D. A. Siegel, and U. Passow. 2023. The importance of transparent exopolymer particles over ballast in determining both sinking and suspension of small particles during late summer in the Northeast Pacific Ocean. Element. Sci. Anthrop. **11**.

Sherr, E. B., and B. F. Sherr. 2007. Heterotrophic dinoflagellates: A significant component of microzooplankton biomass and major grazers of diatoms in the sea. Mar. Ecol. Prog. Ser. **352**: 187–197.

Siegel, D. A., T. DeVries, I. Cetinić, and K. M. Bisson. 2023. Quantifying the ocean's biological pump and its carbon cycle impacts on global scales. Ann. Rev. Mar. Sci. **15**: 329–356.

Siegel, D., and others. 2024. Dynamics of aggregates and sinking carbon fluxes in a turbulent ocean. EarthArXiv Eprints. doi:10.31223/X58709

Smetacek, V. S. 1985. Role of sinking in diatom life-history cycles: Ecological, evolutionary and geological significance. Mar. Biol. **84**: 239–251.

Strickland, J. D. H. 1972. A practical handbook of seawater analysis. Fish Res Board Canada. 310.

Takeuchi, M., M. J. Doubell, G. A. Jackson, M. Yukawa, Y. Sagara, and H. Yamazaki. 2019. Turbulence mediates

marine aggregate formation and destruction in the upper ocean. Sci. Rep. **9**: 16280.

Tiselius, P., and M. Kuylenstierna. 1996. Growth and decline of a diatom spring bloom phytoplankton species composition, formation of marine snow and the role of heterotrophic dinoflagellates. J. Plankton Res. **18**: 133–155.

Tréguer, P., Nelson, D.M. and Brzezinski, M.A. 1992. Protocol for determination of biogenic and lithogenic silica in particulate matter. SO-JGOFS core parameter, int. Rep, 4.

Acknowledgments

The authors are grateful to the EXPORTS science team for the collaborative effort, data and ideas exchange and scientific production that acted as a baseline for the present work. A big thanks goes to the captain and crew of the RRS James Cook. We also thank Dr. Chelsey Baker and Jack Williams who analyzed the TEP samples. Finally, we thank Dr. Mark Brzezinski for the valuable discussions during the preparation of the manuscript. ER, SLG, and DAS were supported by NASA, 80NSSC17K0692. ME was supported by NASA, 80NSSC21K0015. UP was supported by the Canada Research Chairs Program and the Northwest Atlantic Biological Carbon Pump project of the Ocean Frontiers Institute.

Conflict of Interest

None declared.

Submitted 11 January 2024
Revised 12 July 2024
Accepted 05 October 2024

Associate editor: Anja Engel